

# Engineered Core-Shell Magnetic Nanoparticle for MR Dual-Modal Tracking and Safe Magnetic Manipulation of Ependymal Cells in Live Rodents

*Yung-Kang Peng<sup>1,4</sup>, Cathy N. P. Lui<sup>2,4</sup>, Yu-Wei Chen<sup>3</sup>, Shang-Wei Chou<sup>3</sup>, Pi-Tai Chou<sup>3</sup>, Ken K.L. Yung<sup>2\*</sup> and S.C. Edman Tsang<sup>1,4\*</sup>*

<sup>1</sup>Department of Chemistry, University of Oxford, Oxford OX1 3QR, UK

<sup>2</sup>Department of Biology, Hong Kong Baptist University, Hong Kong

<sup>3</sup>Department of Chemistry, National Taiwan University, Taipei, Taiwan

<sup>4</sup>Applied Biology and Chemical Technology, Hong Kong Polytechnics University, Hong Kong

<sup>†</sup>The authors contributed equally to this work.

Correspondences: Ken K.L. Yung: [kklyung@hkbu.edu.hk](mailto:kklyung@hkbu.edu.hk) and S.C. Edman Tsang: [edman.tsang@chem.ox.ac.uk](mailto:edman.tsang@chem.ox.ac.uk)

**KEYWORDS:** *Magnetic field engineering, T<sub>1</sub>-T<sub>2</sub> dual MR imaging, Neural stem cells, Cell harvesting, Safe magnetic manipulation*

## Abstract

Tagging recognition group(s) on superparamagnetic iron oxide is known to aid localization (imaging), stimulation and separation of biological entities using magnetic resonance imaging (MRI) and magnetic agitation/separation (MAS) techniques. Despite the wide applicability of iron oxide nanoparticles in T<sub>2</sub>-weighted MRI and MAS, the quality of the images and safe manipulation of the exceptionally delicate neural cells in a live brain are currently the key challenges. Here, we demonstrate the engineered manganese oxide clusters-iron oxide core-shell nanoparticle as an MR dual-modal contrast agent (DMCA) for neural stem cells imaging and magnetic manipulation in live rodents. As a result, using this engineered nanoparticle and associated technologies, identification, stimulation and transportation of labelled potentially multipotent neural stem cells from a specific location of a live brain to another by magnetic means for self-healing therapy can therefore be made possible.

## 1. Introduction

The potential regenerative effect of neural stem cells for the repair or the replacement of damaged or malfunctioned brain cells has been considered as an appealing strategy due to the limited therapeutic options for some incurable brain diseases, such as Alzheimer's disease and Parkinson's disease, which involve massive cell loss.<sup>[1-3]</sup> The development of stem-cell-based therapies becomes an exciting and fast moving trend in the field. However, the sources of stem cells have given rise to much of controversy. Embryonic stem cell (ESCs) and induced pluripotent stem cell (iPSCs) have shown an outstanding potential in differentiation into specialized cells of all three germ layers, *i.e.* ectoderm, mesoderm and endoderm.<sup>[4-6]</sup> Given that the pluripotency of stem cells can provide a great

impact to clinical applications, it constantly triggers substantial concerns on ethical and immunogenicity matters.<sup>[7-9]</sup> The safety of these cells in therapeutic uses should be carefully evaluated. To develop an effective and safe stem cell-based therapy, adult autologous neural stem cells (NSCs) offer us an alternative and promising candidate in all aspects of function and potential.

The recent discovery of the adult neurogenesis gives strong evidence of the existence of functional neural stem cells (NSCs) in adulthood.<sup>[10,11]</sup> The multipotent adult NSCs were capable of self-renewing and continuously generating different neuronal phenotypes in the ventricular-subventricular zone (V-SVZ) and subgranular zone (SGZ) of the hippocampus.<sup>[10-12]</sup> Notably, V-SVZ is the largest adult neurogenic niche with a special cytoarchitecture for producing olfactory bulb interneurons and oligodendrocytes.<sup>[13-16]</sup> Fe<sub>3</sub>O<sub>4</sub> NPs tagged with recognition groups are commonly used for isolation, pre-concentration and separation of biological entities for a wide range of in-vitro and in-vivo applications. Recently, upon their tagging with the heat sensitive capsaicin receptor wireless magnetothermal agitation to create deep brain stimulation for neurological disorders has also been demonstrated.<sup>[17]</sup> In our early work,<sup>[18]</sup> we demonstrated magnetic (Fe<sub>3</sub>O<sub>4</sub>) nanoparticle (NPs) tagged with anti-CD133 antibody, which successfully extracted cells with CD133 positive (CD133<sup>+</sup>) NSCs from the ependymal layers lining of the V-SVZ in adult rodents by using magnetic separation (MAS). As Fe<sub>3</sub>O<sub>4</sub> NPs can also be used as T<sub>2</sub> agents in clinical magnetic resonance imaging (MRI), we further studied the extracting process of CD133<sup>+</sup> NSCs by T<sub>2</sub>-weighted MRI.<sup>[19]</sup>

However, the induced long range magnetic field of T<sub>2</sub> CA and the susceptibility artifacts distort the MR background image, which commonly masks the fine detail required for clinical diagnosis in T<sub>2</sub>-weighted MRI.<sup>[20]</sup> Also, such single mode contrast is not yet perfect and is increasingly facing challenges especially when more accurate imaging of small biological targets with sufficient background contrast is needed. On the other hand, for magnetic induced agitation and separation (MAS), perhaps, the most serious problems are the extensive damage to the tagged delicate tissues in proximity to the Fe<sub>3</sub>O<sub>4</sub> NPs under the external magnetic field. A severe damage to the tagged V-SVZ was found using Fe<sub>3</sub>O<sub>4</sub>-based T<sub>2</sub> CA after the MRI scan presumably due to the field generated by the MRI (4.7-Tesla).<sup>[21]</sup> This result rises concern about the safety of those recognition group conjugated Fe<sub>3</sub>O<sub>4</sub>-based CA under strong external magnetic fields especially for in-vivo MRI in delicate tissues or organs such as the brain. Despite the wide applicability of iron oxide NPs in T<sub>2</sub>-weighted MRI and MAS, their quality of image and safe manipulation from the live subject are currently the key challenges.<sup>[22,23]</sup> This is especially important for neurological applications due to the uneven distribution of NSCs in structurally complex brain tissue and the exceptionally delicate nature of the neighbor neural cells in a live brain.

To address the above technical difficulties from the contrast agent side, we have recently demonstrated the concept of spatial arrangement of core  $\text{Fe}_3\text{O}_4$  ( $T_2$  component) and  $\text{MnO}$  ( $T_1$  component) in a single core-shell DMCA providing balanced  $T_1/T_2$  in-vivo MR imaging of living ependymal brain cells of rodents with no observed local damage under a MR magnetic field.<sup>[21]</sup> To further explore the potential of this engineered DMCA, in this study, we have monitored the time course distribution of  $\text{CD133}^+$  NSCs by  $T_1/T_2$  MR dual modes and carried out the magnetic isolation process of targeted stem cells in living rat brains. The attached cells are progressively released from the endothelial lining before their extraction from the suspension in cerebrospinal fluid (CSF) either by a syringe or by attachment on a neodymium magnet probe. Gene expression analysis using semi-quantitative RT-PCR including some key transcription factors (Sox2, Nanog and Oct4) for neural stem cell identity is clearly confirmed in both dissected V-SVZ tissue and the DMCA tagged cells. It should be noted that even though the  $\text{MnO}/\text{Fe}_3\text{O}_4$   $T_1$ - $T_2$  DMCA<sup>[24,25]</sup> or related kinds of DMCA<sup>[26-29]</sup> have been used in *in vivo* imaging, no further progress has been reported on their applications in neural stem cells imaging and magnetic manipulation in live rodent especially for this engineered DMCA with balanced  $T_1/T_2$ .

## 2. Methods

**Synthesis of  $\text{Fe}_3\text{O}_4@\text{MnO}/\text{SiO}_2$  NPs.** The  $\text{Fe}_3\text{O}_4@\text{MnO}/\text{SiO}_2$  was prepared according to our previous report.<sup>[21]</sup> Briefly, for the coating of mesoporous silica shell on as-prepared  $\text{Fe}_3\text{O}_4$  NP, 2 ml of  $\text{Fe}_3\text{O}_4$  NP (10 mg/ml in chloroform) were mixed with 300 mg of CTAB and 20 ml of deionized water. The mixture was then stirred vigorously until the formation of the oil-in-water microemulsion appeared with a turbid brown solution. The chloroform solvent was boiled off from the solution, resulting in a transparent brown  $\text{Fe}_3\text{O}_4/\text{CTAB}$  solution. This solution was added to a mixture of 29.5 mL of water and 0.5 mL of 0.8 M NaOH solution, and the mixture was heated. At approximately 60°C under stirring, 0.5 mL of TEOS and 3 mL of ethyl acetate were loaded to the reaction solution in sequence. The solution was stirred for another 6 h and the resulting product,  $\text{Fe}_3\text{O}_4@\text{SiO}_2$ , was washed by ethanol/water several times and collected by centrifugation (14500 rpm, 10 min). The as-prepared  $\text{Fe}_3\text{O}_4@\text{SiO}_2$  nanoparticles were used as template for the synthesis of ultrasmall  $\text{MnO}$  NPs (embedded in  $\text{mSiO}_2$ ). Typically, 30 mg of  $\text{Fe}_3\text{O}_4@\text{SiO}_2$  NPs (30 mg), 660 mg of  $\text{MnCl}_2 \cdot 4\text{H}_2\text{O}$  (99%, Aldrich) and 10 mL of triethylene glycol (99%, Sigma-Aldrich) were added to a 50 mL three-necked flask and the mixture was magnetically stirred. The reaction temperature was then raised to 200 °C and kept at that temperature for 6 h before cooling to room temperature. The solvent, unreacted coating ligand, unreacted  $\text{Mn}^{2+}$ , and  $\text{Cl}^-$  ions were removed from the reaction solution by

centrifugation (14500 rpm, 10 min). The product,  $\text{Fe}_3\text{O}_4@\text{MnO}/\text{SiO}_2$  NPs were washed with deionized water three times.

**Amine Modification, CTAB removal and CD133 Immobilization.** To immobilize CD133 antibody on  $\text{Fe}_3\text{O}_4@\text{MnO}/\text{SiO}_2$  NPs, amine modification was firstly carried out followed by CTAB removal.<sup>[18,19]</sup> Briefly, 3-amino-propyltrimethoxysilane (95%, Acros) (10  $\mu\text{L}$ ) was added to a mixture of ethanol (30 mL), DI water (6 mL),  $\text{NH}_4\text{OH}$  (300  $\mu\text{L}$ ), and as-prepared NPs (20 mg). After 24 h of reaction, the product,  $\text{Fe}_3\text{O}_4@\text{MnO}/\text{SiO}_2\text{-NH}_2$ , was collected by centrifugation and washed with DI water for several times. Template molecules, CTAB, were removed *via* a fast and efficient ion exchange method. The NPs were transferred to 50 mL of ethanol containing 0.3 g of  $\text{NH}_4\text{NO}_3$  ( $\geq 99.0\%$ , Aldrich) and kept at  $60^\circ\text{C}$  for 2 h. After 6 h of dialysis, the product (without CTAB) was prepared and ready for use. The anti-CD133 antibodies (Milteny Biotec) were covalently conjugated onto  $\text{Fe}_3\text{O}_4@\text{MnO}/\text{SiO}_2\text{-NH}_2$  (16 mg) by incubating with 10 mg N-(3-dimethylaminopropyl)-N'-ethylcarbodiimide hydrochloride (EDC, Aldrich) and 10 mg N-hydroxysuccinimide (NHS, 98%, Acros) for 30 min. The anti-CD133 antibodies (1 mL) were then added to the mixture and incubated for another 1 h at room temperature. The antibody-conjugated nanocomposites,  $\text{Fe}_3\text{O}_4@\text{MnO}/\text{SiO}_2\text{-CD133}$ , were purified by centrifugation (14500 rpm, 10 min) and washed 3 times with PBS (pH 7.4).

**In Vivo MRI Experiments.** Adult Sprague-Dawley (SD) rats (8 weeks of age, male, body mass  $\sim 300$  g) were employed in the experiments. All the animals were fully anesthetized with 5% isoflurane at  $1\text{ L min}^{-1}$  air flow and fitted with a custom designed head holder inside the magnet of a 4.7-Tesla Biospec 47/40 MR scanner. 1–1.5% isoflurane was maintained at  $1\text{ L min}^{-1}$  air flow throughout the whole experiments. The MRI experiments were performed before and at different times after the injection of three different CAs ( $T_1$  CA,  $T_2$  CA, DMCA) at a dose of  $0.19\text{ mg kg}^{-1}$  with ( $T_1/T_2$ ) TR = 500/5000 ms, ( $T_1/T_2$ ) TE<sub>eff</sub> = 8/70 ms, FOV =  $7\text{ cm} \times 7\text{ cm}$ , slice thickness = 1.3 mm, and matrix size =  $256 \times 128$  (zero-padded to  $256 \times 256$ ) with six repetitions. This concentration of magnetic nanoparticle (i.e. about  $2000\text{ }\mu\text{g/mL}$ ) was found to be effectively in isolating the ependymal cells by external magnetic field<sup>[18]</sup>. It took around 20 mins for acquiring both  $T_1$ - and  $T_2$ -weighted MR scans at the three periods of time (i.e. 1h, 6h and 24h after injection).

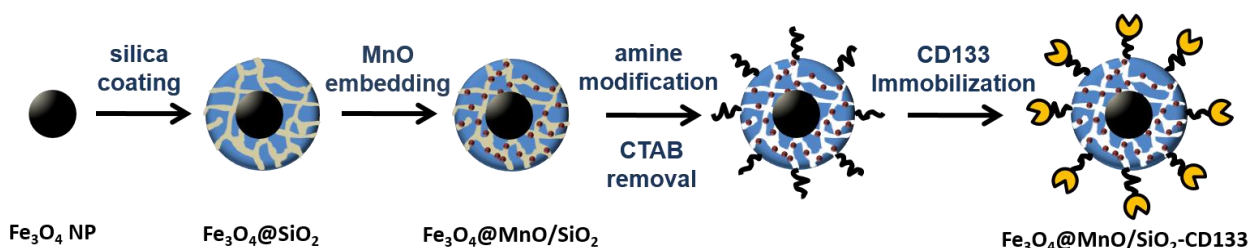
**Immunostaining and Reverse Transcription-Polymerase Chain Reaction.** The animals were deeply anesthetized with an overdose of sodium pentobarbital (60 mg/kg, i.p., Saggital) and perfused transcardially with fixative (3 % paraformaldehyde with 0.1% glutaraldehyde solution in 0.1 M phosphate buffer (PB), pH 7.4) by using a peristaltic pump. The brain was then cut into  $70\text{ }\mu\text{m}$  sections by using vibratome. Immunofluorescence experiment was performed to label the CD133-expressing NSCs and Glial fibrillary acidic protein (GFAP)-expressing SVZ astrocytes under the laser scan confocal microscope (Olympus fluoview 1000). The harvested  $\text{CD133}^+$  NSCs were

collected by magnetic agitation and the total RNA extraction was prepared by a miniprep system (Promega). Reverse transcription polymerase chain reaction (RT-PCR) was then carried out for the determination of the expressions of Sox2, Nanog and Oct4. GAPDH was used as a housekeeping gene for positive control.

**LDH Cytotoxicity Assay.** The primary CD133 positive astrocytes were collected from P0-1 rats. LDH assay was performed to investigate the toxicity of the NPs. A serial concentration of NPS ranging from 200 to 5000 mg/mL was prepared. 50 uL of cell and 50 uL reaction mixtures were transferred to the 96 well plate. After 30 minutes of incubation, another 50 uL of stop solution was added. The absorbance at 490 nm and 680 nm were measured for the LDH activity.

### 3. Results

#### Preparation and characterization of dual-modal contrast agents.



**Scheme 1.** Illustration of the synthetic protocols of CD133-tagged DMCA ( $\text{Fe}_3\text{O}_4@\text{MnO}/\text{SiO}_2\text{-CD133}$ ).

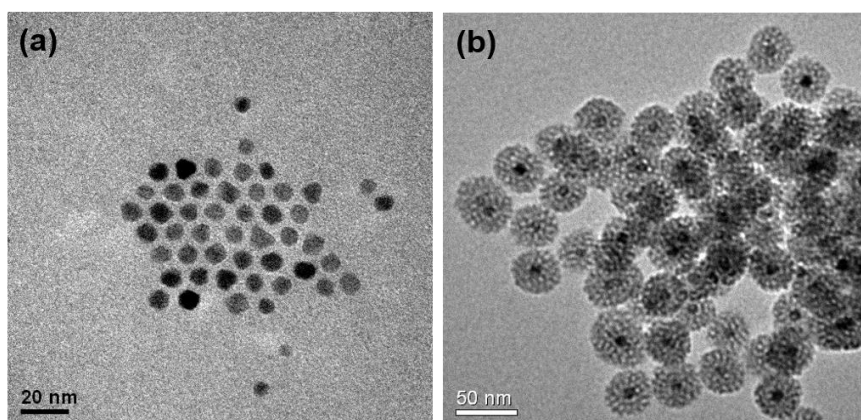


**Figure 1.** TEM images of (a)  $\text{Fe}_3\text{O}_4$  NPs and (b) DMCA ( $\text{Fe}_3\text{O}_4@\text{MnO}/\text{SiO}_2$ ).

The procedure to prepare the final DMCA particle ( $\text{Fe}_3\text{O}_4@\text{MnO}/\text{SiO}_2\text{-CD133}$ ) from hydrophobic  $\text{Fe}_3\text{O}_4$  NPs to  $\text{Fe}_3\text{O}_4@\text{SiO}_2$  to  $\text{Fe}_3\text{O}_4@\text{MnO}/\text{SiO}_2$  is the same as our previous report.<sup>[21]</sup> Details are elaborated in experimental section (Scheme 1). Briefly, as-prepared 8 nm  $\text{Fe}_3\text{O}_4$  NPs (Figure 1a) were transferred to the aqueous phase by utilizing cetyltrimethylammonium bromide (CTAB). In the subsequent sol-gel reaction, the silica-CTAB layer is formed locally around the CTAB- $\text{Fe}_3\text{O}_4$  NPs under basic conditions through an electrostatic interaction between the cationic



(CTAB) and anionic (silicate) species. The mesoporous shell of the product,  $\text{Fe}_3\text{O}_4@\text{SiO}_2$ , was used as a template for the embedding of ultrasmall MnO NPs. The TEM image and HRTEM of the resulting product,  $\text{Fe}_3\text{O}_4@\text{MnO}/\text{SiO}_2$ , are shown in [Figure 1b](#) and [Figure S1](#). Accordingly, the MnO/SiO<sub>2</sub> shell of  $\text{Fe}_3\text{O}_4@\text{MnO}/\text{SiO}_2$  is homogeneous (thickness ~19.5 nm) and the lattice fringes of  $\text{Fe}_3\text{O}_4$  and MnO NPs can be clearly characterized. The XRD measurement ([Figure S2](#)) reveals a broad peak at  $2\theta = 23$  degrees (from amorphous silica) while no peak of MnO NPs was observed presumably due to their extremely small particle size. The iron, manganese and silicon content of  $\text{Fe}_3\text{O}_4@\text{MnO}/\text{SiO}_2$  was verified using energy-dispersive X-ray (EDX) spectroscopy ([Figure. S3](#)). The magnetic properties of  $\text{Fe}_3\text{O}_4@\text{MnO}/\text{SiO}_2$  were assessed by SQUID ([Figure S4](#)). Compared to  $\text{Fe}_3\text{O}_4@\text{SiO}_2$  (~1.5 emu/g at 300K), the saturation magnetization of  $\text{Fe}_3\text{O}_4@\text{MnO}/\text{SiO}_2$  drops to ~1 emu/g at 300K which is attributed to the embedding of paramagnetic MnO clusters in the mesoporous shell. As the net magnetization ( $M_z$ ) is strongly related to the transverse relaxivity ( $r_2$ ) ( $M_z \propto r_2$ ), a decrease in  $r_2$  value from 109.31 to 93.15  $\text{mM}^{-1}\text{s}^{-1}$  after the introduction of MnO clusters ([Table S1](#)). The incorporation of these T<sub>1</sub> materials also doubled the  $r_1$  value (from 1.15 to 2.17  $\text{mM}^{-1}\text{s}^{-1}$ ) and thus a reduced  $r_2/r_1$  ratio from 94.94 to 42.93 was obtained ([Table S1](#)). The corresponding MR phantom imaging study ([Figure S5](#)) provides further evidence that  $\text{Fe}_3\text{O}_4@\text{SiO}_2$  exhibit typical T<sub>2</sub> characteristics. While the  $\text{Fe}_3\text{O}_4@\text{MnO}/\text{SiO}_2$  particle, with lower  $r_2/r_1$  ratios, shows MR signals in both T<sub>1</sub>- and T<sub>2</sub>-weighted imaging. To immobilize the CD133 antibody on  $\text{Fe}_3\text{O}_4@\text{MnO}/\text{SiO}_2$  NPs, amine modification was firstly carried out followed by CTAB removal. The anti-CD133 antibodies were then covalently conjugated onto the silica surface by EDC (N-(3-dimethylaminopropyl)-N'-ethylcarbodiimide hydrochloride)/NHS (N-hydroxysuccinimide) coupling. See reference 21 for comprehensive particle characterization and relevant in-vitro MR experiment.

## **In Vivo Experiments.**

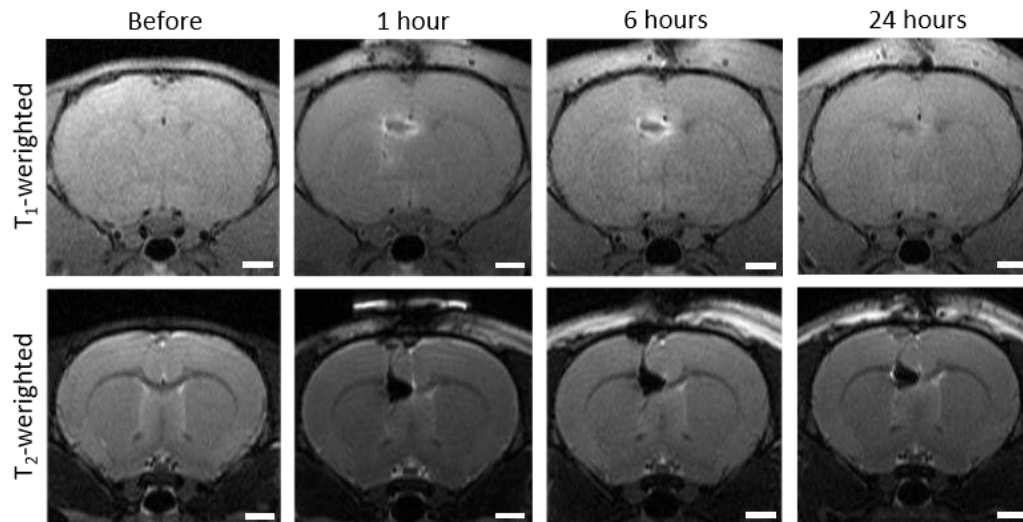


**Figure 2.** A time course  $T_1$ -weighted and  $T_2$ -weighted images (scale bar: 2 mm) of labelled CD133<sup>+</sup> NSCs from the choroid plexus lining along the V-SVZ after the injection of DMCA ( $\text{Fe}_3\text{O}_4@\text{MnO}/\text{SiO}_2\text{-CD133}$ ) in rat brain at different time intervals (1 hour, 6 hours and 24 hours).

We unilaterally injected 5  $\mu\text{L}$  of DMCA ( $\text{Fe}_3\text{O}_4@\text{MnO}/\text{SiO}_2\text{-CD133}$ ) (2000  $\mu\text{g mL}^{-1}$  in PBS solution) into the left V-SVZ of the rat brains by a micro-syringe through a preformed hole on their skulls by micro-surgery. As shown in [Figure 2](#), DMCA particles clearly allow a time course  $T_1$ - $T_2$  signals of the regions of interest in a live rat brain at different selected time intervals (1 h, 6 h and 24 h). With the conjugation of CD133 antibodies, DMCA could specifically localize to CD133<sup>+</sup> NSCs of the V-SVZ linings and no dispersal of the particles could be observed in the brain fluid or other parts of the brain, 1 h after the injection. An extensive binding of the antibodies to the cells could be observed at the 6 h incubation time: a spatial distribution of the injected DMCA could be visualized ([Figure 2](#) and [Figure S6](#)). The highest contrast was confined only to the ventricular surface of V-SVZ, indicating that the contrast agent could preferentially bind to the ependymal. No detectable signals were shown in the ventricular lumen of V-SVZ or other brain areas ([Figure S6](#)). Upon injection, it is envisaged that selective binding and removal of labels/cells from the superficial endothelial linings of SVZ with a clear evidence of internalization are both taken place, which are rather dynamic in a rat body ([Figure 3](#)).

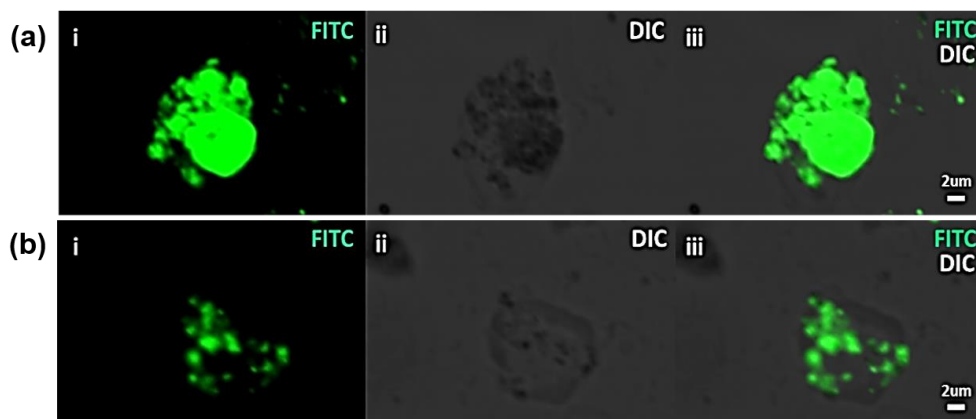


**Figure 3.** The internalization of DMCA ( $\text{Fe}_3\text{O}_4@\text{MnO}/\text{SiO}_2\text{-CD133}$ ) was monitored by confocal microscopic examination of the localization of DMCA (FITC dye included) on the NSCs. Images collected (a) 6 hours and (b) 24 hours after the injection respectively. Fewer particles were bound on the cells and the uptake of the DMCA was observed after 24 hours.

A time course  $T_1$ - $T_2$  signal intensity of left and right (control) ventricles in the rat brain at different time intervals (1 hour, 6 hours and 24 hours) is shown in [Figure 4](#). Clearly, an induction time was required for the diffusion and binding process but a significantly lower yield was obtained at the end of the 24-hour incubation. The drop of the signals indicated the low risk of the accumulation which might evoke unwanted health problems. The final clearance of most particles can be evidenced by the Prussian blue staining experiment 2 days after injection ([Figure S7](#)). All animals were alive and apparently healthy even after receiving repeated MRI scanning. It is noted that both  $T_1$  and  $T_2$  signals still remain 24 hr after injection ([Figure 4](#)). However, the  $T_2$  signal (from iron oxide part of  $\text{Fe}_3\text{O}_4@\text{MnO}/\text{SiO}_2\text{-CD133}$ ) was less sensitive compared to  $T_1$  signal. The difference in sensitivity between  $T_1$  and  $T_2$ -weighted imaging has long been known to be due to different relaxation mechanisms.<sup>[20]</sup> As  $T_2$  CAs are superparamagnetic based iron oxide nanoparticles, they generate an induced magnetic field under an external field, perturbing the spin-spin relaxation ( $T_2$ ) processes of protons in the vicinity and giving rise to negative (dark) MRI images. Since this relaxation is induced through space by the inhomogeneity of the local magnetic field, an observable  $T_2$  signal can thus be generated with a low dose of  $T_2$  CAs. However, the induced long-range magnetic field not only perturbs neighbouring normal tissues but also distorts the background image (the blooming effect).<sup>[20]</sup> This could become the main obstacle to diagnosing the exact locations of lesions. In stark contrast, even though the spin-lattice relaxation ( $T_1$ ) can give a positive (bright) MR image, it needs direct contact between the paramagnetic centre and the water molecule in the inner coordination sphere.<sup>[30,31]</sup> The  $T_1$  signal is thus very sensitive to the degrees of water penetration to the inner paramagnetic center and could disappear if the diffusion of water is blocked. Accordingly,  $T_1$ -weighted imaging is much more sensitive to the local environment compared to  $T_2$ -weighted imaging.



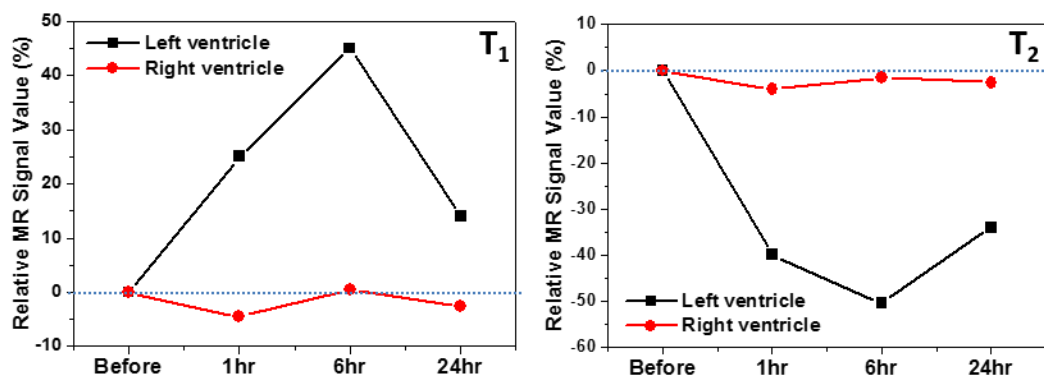


**Figure 4.** A time course  $T_1$ - $T_2$  signal intensity of left and right (control) ventricles in rat brain at different time intervals (1 hour, 6 hours and 24 hours).

We are at present unable to give the number of magnetic NPs that are attaching to each NSC. It is evident that the process of attachment of ependymal cells by magnetic NPs is rather dynamic in a living subject. They continue to attach and detach in a flowing fluid and can also be taken up by inner cells. Several processes have to be considered: (1) the diffusion and adsorption of particles on NSCs, (2) the removal of particles by CSF, (3) dynamically binding/(4) unbinding to NSCs and (5) the internalization of bound particles by NSC. The dynamic process of these steps can be visualized by the time course MRI  $T_1$ - $T_2$  signal intensity shown in Figure 4. A 6 hour induction time was required for the diffusion and binding process to reach high contrast under MRI  $T_1$  (Figure 4a) and  $T_2$  mode (Figure 4b). Later, the decrease of both signals can be attributed to the higher rate of particle removal (processes 2 and 4) compared to the counter processes (1), (3) and (5).

#### Immunostaining and Reverse Transcription-Polymerase Testing.

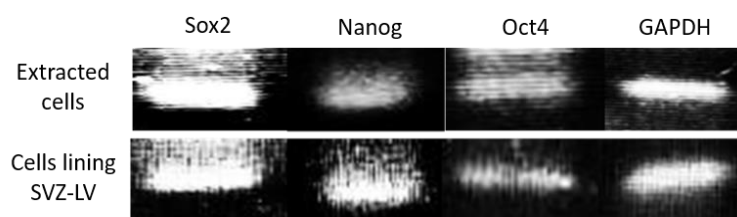


**Figure 5.** Gene expression analysis was investigated with semi-quantitative RT-PCR.<sup>[32]</sup> The key transcription factors (Sox2, Nanog and Oct4) for stem cell identity were expressed in both the dissected V-SVZ tissue and the DMCA ( $\text{Fe}_3\text{O}_4@\text{MnO}/\text{SiO}_2\text{-CD133}$ ) NPs tagged cells. It is noted that this is a semi-quantitative analysis and the bands for assaying the same gene but from different samples cannot be compared directly.

To address whether the extracted cells possess stemness characteristics, we have previously cultured the magnetic isolated cells (collected by DMCA NPs) to neurospheres and differentiated them into different phenotypes.<sup>[18]</sup> Herein, we further elucidate the potency of the extracted cells. Sox2, Nanog and Oct4 were well-considered as the key transcription factors for the stem cell identity.<sup>[32]</sup> Given the notion that the expression of these defined transcription factors could regulate

the signalling pathways on self-renewal and proliferation for a pluripotent phenotype, we collected the ependymal tissue from the walls of V-SVZ by dissection and compared their gene expressions with the ones of the extracted cells. As expected, RT-PCR analysis (Figure 5) clearly shows: (a) both CD133<sup>+</sup> cells extracted and cells directly from SVZ regions displayed the Sox2, Nanog and Oct4 where CD133 appeared to act as the biomarkers for the NSCs. (b) When subject to the PCR assays, the starting cell numbers in the two above categories were not exactly the same, as they were obtained by different methods (directly peeling from lateral ventricle and extracting by DMCA). Although the same amplification cycles for both categories were used, the DNA copy number after amplification might not be the same among the two categories of cells. (c) Both categories of cells displayed the three genes which confirmed their identities. The cytotoxicity of DMCA NPs to those extracted CD133 positive primary astrocytes was evaluated by LDH cytotoxicity assay. As shown in Figure S8, the cell viability can still be maintained at around 80% with the concentration of DMCA NPs up to 5000 µg/mL.

#### 4. Discussion

The in-situ labelling and MR tracking of micron-sized particles of iron oxide (MPIOs)<sup>[22]</sup> or superparamagnetic iron oxide nanoparticles (SPIONs)<sup>[23]</sup> by injecting them into the lateral ventricle of a subject have been reported previously. However, limitations such as significant image distortion, non-targeting nature and low labelling efficiency were observed and can be largely derived from inappropriate uses of the imaging particle reagents. For example, the major drawback of using those pure iron oxide particle as T<sub>2</sub>-weighted MR contrast agent with or without the antibody is its intrinsically high magnetic susceptibility. This can induce a long-range magnetic field perturbing the neighbouring normal tissues and also distorting the background image<sup>[20]</sup> causing an obstacle to tracking the migration of NSCs in this area. A similar MR result was also observed in our previous study using CD133 tagged iron oxide nanoparticles for the in situ study (MR T<sub>2</sub>-weighted imaging) of neural stem cell harvesting.<sup>[19]</sup>

To address these problems, T<sub>1</sub> contrast agents seem to be an advantageous alternative as they can provide positive (bright) MRI images and, most importantly, no distortion of the background.<sup>[33]</sup> Since the T<sub>2</sub>-component, iron oxide, is necessary here, in an aim to extract CD133<sup>+</sup> NSCs in SVZ by magnetic separation, we have engineered DMCA by integrating both T<sub>2</sub> and T<sub>1</sub> components into a single nanoparticle with suitable magnetization.<sup>[21]</sup> According to the in vivo testing, the T<sub>1</sub>-weighted MR imaging indeed showed a better resolution, without background distortion, compared to the T<sub>2</sub>-weighted MR imaging (Figure 2). In the meantime, milder magnetic agitation can assist the

separation of these magnetic tagged NSCs without inflicting observable local damage under the magnetic field from the MRI equipment. Regarding the low cell labelling efficiency encountered before,<sup>[22,23]</sup> Koretsky's group<sup>[22]</sup> used bare MPIOs without antibody conjugation, while Shen's group<sup>[23]</sup> adopted an inappropriate antibody conjugation (CD15) on SPIONs. According to literature,<sup>[34]</sup> CD15 can hardly be regarded as a specific "marker" for NSC but more suitable as a specific marker for myeloma cells. The more specific and higher efficiency of the NPs conjugated with antibody CD133 on cell labelling have been demonstrated in our previous report<sup>[18,19,21]</sup> (see ref.21 for control experiment carried out for DMCA without CD133 modification), which enabled the isolation of the whole single cell layer of NSCs by magnetic agitation. Overall, there are limitations to the in-situ method that we employed in this work, however, the preliminary study presented here using this strategy shows clearly that the significant image distortion, non-targeting nature and low labelling efficiency can be much alleviated through using our engineered DMCA.

## 5. Conclusions

We believe that this engineered nanoparticle and associated technologies may have significant implications in safely isolating and relocating individual patients' own autologous neural stem cells for tailor-made treatments of their specific neurological problems in future stem cells therapy without encountering ethical issues and risk of immune response. All the subjects have remained alive and showed no signs of neurological symptoms despite receiving the above treatments. This conclusion, although presently demonstrated for imaging and isolation of CD133<sup>+</sup> NSCs in a live rodent brain, would be expected to be transferable to other delicate cellular inclusions to organ levels. It is thus believed that this capability can offer a stepping stone to lead to rational engineering of functional DMCA NPs for a wide range of accurate magnetic manipulations and can be safely applied to patients in the future.

## Acknowledgement

We thank the EPSRC of UK for funding of this project. YKP acknowledges the University of Oxford Clarendon Fund Scholarship for his DPhil study. YKP and SCET are grateful to HKPU for the academic visiting scheme to partially support this work. CNPL and KKLY are grateful to NFSC and HKBU for funding support. We also thank KE and YA from Chinese University of HK for the support in Prussian blue staining experiment. We are indebted to the support from Taiwan Mouse Clinic which is currently funded through the National Research Program for Biopharmaceuticals

(NRPB) at the Ministry of Science and Technology of Taiwan, particularly for the MRI mouse experiments presented in this paper.

## References

1. Brettschneider, J.; Tredici, K. D.; Lee, V. M.; Trojanowski, J. Q. Spreading of Pathology in Neurodegenerative Diseases: a Focus on Human Studies. *Nat. Rev. Neurosci.* **2015**, *16*, 109–120.
2. Mattson, M. P.; Magnus, T. Ageing and Neuronal Vulnerability. *Nat. Rev. Neurosci.* **2006**, *7*, 278–294.
3. Mattson, M. P. Pathways Towards and Away from Alzheimer's Disease. *Nature* **2004**, *430*, 631–639.
4. Liang, G.; Zhang, Y. Embryonic Stem Cell and Induced Pluripotent Stem Cell: an Epigenetic Perspective. *Cell Res.* **2013**, *23*, 49–69.
5. Kang, L.; Wang, J.; Zhang, Y.; Kou, Z.; Gao, S. iPS Cells can Support Full-Term Development of Tetraploid Blastocyst-Complemented Embryos. *Cell stem cell* **2009**, *5*, 135–138.
6. Kang, L.; Gao, S. Pluripotency of Induced Pluripotent Stem Cells. *J. Anim. Sci. Biotechnol.* **2012**, *3*, 5.
7. Miura, K.; Okada, Y.; Aoi, T.; Okada, A.; Takahashi, K.; Okita, K.; Nakagawa, M.; Koyanagi, M.; Tanabe, K.; Ohnuki M.; *et al.* Variation in the Safety of Induced Pluripotent Stem Cell Lines. *Nat. Biotechnol.* **2009**, *27*, 743–745.
8. Sim, F. J.; McClain, C. R.; Schanz, S. J.; Protack, T. L.; Windrem, M. S.; Goldman, S. A CD140a Identifies a Population of Highly Myelinogenic, Migration-Competent and Efficiently Engrafting Human Oligodendrocyte Progenitor Cells. *Nat. biotechnol.* **2011**, *29*, 934–941.
9. Vogel, G. Ready or Not? Human ES Cells Head Toward the Clinic. *Science* **2005**, *308*, 1534–1538.
10. Fuentealba, L. C.; Obernier, K.; Alvarez-Buylla, A. Adult Neural Stem Cells Bridge Their Niche. *Cell stem cell* **2012**, *10*, 698–708.
11. Ming, G. L.; Song, H. Adult Neurogenesis in the Mammalian Brain: Significant Answers and Significant Questions. *Neuron* **2011**, *70*, 687–702.
12. Zhao, C.; Deng, W.; Gage, F. H. Mechanisms and Functional Implications of Adult Neurogenesis. *Cell* **2008**, *132*, 645–660.
13. Chiasson, B. J.; Tropepe, V.; Morshead, C. M.; Kooy, D. Adult Mammalian Forebrain Ependymal and Subependymal Cells Demonstrate Proliferative Potential, but Only Subependymal Cells Have Neural Stem Cell Characteristics. *J. Neurosci.* **1999**, *19*, 4462–4471.
14. Coskun, V.; Wu, H.; Blanchi, B.; Tsao, S.; Kim, K.; Zhao, J.; Biancotti, J. C.; Hutnick, L.; Krueger, R. C.; Fan, G.; *et al.* CD133+ Neural Stem Cells in the Ependyma of Mammalian Postnatal Forebrain. *Proc. Natl. Acad. Sci.* **2008**, *105*, 1026–1031.
15. Zhao, C.; Suh, H.; Gage, F. H. Notch Keeps Ependymal Cells in Line. *Nat. Neurosci.* **2009**, *12*, 243–245.
16. Doetsch, F.; Caille, I.; Lim, D. A.; Garcia-Verdugo, J. M.; Alvarez-Buylla, A. Subventricular Zone Astrocytes are Neural Stem Cells in the Adult Mammalian Brain. *Cell* **1999**, *97*, 703–716.
17. Chen, R.; Romero, G.; Christiansen, M. G.; Mohr, A.; Anikeeva, P. Wireless Magnetothermal Deep Brain Stimulation, *Science* **2015**, *347*, 1477–1480.
18. Lui, C. N. P.; Tsui, Y. P.; Ho, A. S. L.; Shum, D. K. Y.; Chan, Y. S.; Wu, C. T.; Li, H. W.; Tsang, S. C. E.; Yung, K. K. L. Neural Stem Cells Harvested from Live Brains by Antibody-Conjugated Magnetic Nanoparticles. *Angew. Chem. Int. Ed.* **2013**, *52*, 12298–12302.

19. Peng, Y.-K.; Lui, C. N. P.; Lin, T.-H.; Chang, C.; Chou, P.-T.; Yung, K. K. L.; Tsang, S. C. E. Multifunctional Silica-Coated Iron Oxide Nanoparticles: a Facile Four-in-One System for In Situ Study of Neural Stem Cell Harvesting. *Faraday Discuss.* **2014**, *175*, 13–26.
20. Jun, Y. W.; Lee, J. H.; Cheon, J. Chemical Design of Nanoparticle Probes for High-Performance Magnetic Resonance Imaging. *Angew. Chem. Int. Ed.* **2008**, *47*, 5122–5135.
21. Peng, Y.-K.; Lui, C. N. P.; Chen, Y.-W.; Chou, S.-W.; Raine, E.; Chou P.-T.; Yung, K. K. L.; Tsang, S. C. E. Engineering of Single Magnetic Particle Carrier for living Brain cell imaging: A Tunable T<sub>1</sub>-/T<sub>2</sub>-Dual-Modal Contrast Agent for Magnetic Resonance Imaging application (MRI). *Chem. Mater.* **2017**, *29*, 4411–4417.
22. Sumner, J. P. S.; Shapiro, E. M.; Maric, D.; Conroy, R.; Koretsky, A. P. In Vivo Labeling of Adult Neural Progenitors for MRI with Micron Sized Particles of Iron Oxide: Quantification of Labeled Cell Phenotype. *NeuroImage* **2009**, *44*, 671–678.
23. Zhong, X.-M.; Zhang, F.; Yang, M.; Wen, X.-H.; Zhang, X.; Duan, X.-H.; Shen, J. In Vivo Targeted Magnetic Resonance Imaging of Endogenous Neural Stem Cells in the Adult Rodent Brain. *Biomed. Res. Int.* **2015**, *2015*, 131054.
24. Im, G. H.; Kim, S. M.; Lee, D.-G.; Lee, W. J.; Lee, J. H.; Lee, I. S. Fe<sub>3</sub>O<sub>4</sub>/MnO hybrid nanocrystals as a dual contrast agent for both T<sub>1</sub>- and T<sub>2</sub>-weighted liver MRI. *Biomaterials* **2013**, *34*, 2069–2076.
25. Li, S.; Shao, C.; Gu, W.; Wang, R.; Zhang, J.; Lai, J.; Li, H.; Ye, L. Targeted imaging of brain gliomas using multifunctional Fe<sub>3</sub>O<sub>4</sub>/MnO nanoparticles. *RSC Adv.* **2015**, *5*, 33639–33645.
26. Bae, K. H.; Kim, Y. B.; Lee, Y.; Hwang, J.; Park, H.; Park, T. G. Bioinspired Synthesis and Characterization of Gadolinium-Labeled Magnetite Nanoparticles for Dual Contrast T<sub>1</sub>- and T<sub>2</sub>-Weighted Magnetic Resonance Imaging. *Bioconjugate Chem.* **2010**, *21*, 505–512.
27. Choi, J. S.; Lee, J. H.; Shin, T. H.; Song, H. T.; Kim, E. Y.; Cheon, J. Self-Confirming “AND” Logic Nanoparticles for Fault-Free MRI. *J. Am. Chem. Soc.* **2010**, *132*, 11015–11017.
28. Yanga, H.; Zhuanga, Y.; Sund, Y.; Daia, A.; Shib, X.; Wue, D.; Lid, F.; Hua, H.; Yanga, S. Targeted dual-contrast T<sub>1</sub>- and T<sub>2</sub>-weighted magnetic resonance imaging of tumors using multifunctional gadolinium-labeled superparamagnetic iron oxide nanoparticles. *Biomaterials* **2011**, *32*, 4584–4593.
29. Shin, T.-H.; Choi, J.-S.; Yun, S.; Kim, I.-S.; Song, T.-H.; Kim, Y.; Park, I. K.; Cheon, J. T<sub>1</sub> and T<sub>2</sub> Dual-Mode MRI Contrast Agent for Enhancing Accuracy by Engineered Nanomaterials. *ACS Nano* **2014**, *8*, 3393–3401.
30. Peng, Y.-K.; Lai, C.-W.; Liu, C.-L.; Chen, H.-C.; Hsiao, Y.-H.; Liu, W.-L.; Tang, K.-C.; Chi, Y.; Hsiao, J.-K.; Lim, K.-E.; *et al.* A New and Facile Method to Prepare Uniform Hollow MnO/Functionalized mSiO(2) Core/Shell Nanocomposites. *ACS Nano* **2011**, *5*, 4177–4187.
31. Peng, Y.-K.; Liu, C.-L.; Chen, H.-C.; Chou, S.-W.; Tseng, W.-H.; Tseng, Y.-J.; Kang, C.-C.; Hsiao, J.-K.; Chou, P.-T. Antiferromagnetic Iron Nanocolloids: a New Generation In Vivo T<sub>1</sub> MRI Contrast Agent. *J. Am. Chem. Soc.* **2013**, *135*, 18621–18628.
32. Kim, J. B.; Greber, B.; Araújo-Bravo, M. J.; Meyer, J.; Park, K. I.; Zaehres, H.; Schöler, H. R. Direct Reprogramming of Human Neural Stem Cells by OCT4. *Nature* **2009**, *461*, 649–654.
33. Peng, Y.-K.; Tsang, S. C. E.; Chou, P.-T. Chemical Design of Nanoprobes for T<sub>1</sub>-Weighted Magnetic Resonance Imaging. *MATER. TODAY.* **2016**, *19*, 336–348.
34. Read, T.-A.; Fogarty, M. P.; Markant, S. L.; McLendon, R. E.; Wei, Z.; Ellison, D. W.; Febbo, P. G.; Wechsler-Reya, R. J. Identification of CD15 as a Marker for Tumor-Propagating Cells in a Mouse Model of Medulloblastoma. *Cancer Cell* **2009**, *15*, 135–147.